

Measurement of Proton-Proton Triple Scattering at 430 MeV*

R. ROTH AND E. ENGELS, JR.†
Princeton University, Princeton, New Jersey

AND

S. C. WRIGHT, P. KLOEPPPEL,‡ AND R. HANDLER
University of Chicago, Chicago, Illinois

AND

LEE G. PONDROM‡
Columbia University, New York, New York

The polarization parameters P , D , R , A , and A' have been measured at 7 scattering angles between 30° and 120° in the center-of-mass system with an incident energy of 430 MeV. A 56% polarized beam was prepared by scattering on an internal beryllium target in the Chicago synchrocyclotron. A liquid-hydrogen target was used for the p - p scattering and the outgoing polarization was analyzed with a third scattering in the carbon plates of a spark chamber. The scattering asymmetry ϵ was determined by fitting the data to a distribution $1 + \epsilon \cos \theta$ by the maximum-likelihood method. The analyzing power of the spark chamber as a function of energy was measured in beams of known polarization. The beam polarization before and after the p - p scattering was manipulated with a solenoid and two bending magnets. During a 5-week run, 1.4×10^6 pictures were taken. The pictures were scanned and measured on angular encoding machines with a least count of $\frac{1}{3}$ deg. The measurements are compared with the extrapolations of several phase-shift and resonance analyses of experimental data at higher and lower energies.

I. INTRODUCTION

THIS paper is a continuation of earlier work¹ applying spark-chamber techniques to the study of polarization phenomena in nucleon-nucleon scattering. In I the correlation coefficients C_{NN} and C_{KP} were measured at 400 and 450 MeV for p - p scattering. Here we report measurements of the triple scattering parameters D , R , A and A' at angles between 30° and 120° in the center-of-mass (c.m.) system. These parameters were first proposed in 1954 by Wolfenstein² as a convenient form for the measurable quantities which characterize the spin-dependent aspects of p - p scattering. Since that time there have been fairly complete sets of measurements in the range of c.m. scattering angles 30° - 90° , for incident energies of 140, 210, and 310 MeV, in addition to a few measurements of D and R at other energies.³ The experimental and theoretical progress in nucleon-nucleon scattering is well documented in review articles by Wolfstein,⁴ Hess,⁵ MacGregor, Moravcsik, and Stapp,⁶ Breit,⁷ and Nigam,⁸ and in a book by Wilson.³

The basic detection equipment was the same as that reported in I, namely a carbon-plate spark chamber. The analysis techniques used here were similar to those of I. The important differences were the polarized proton beam and the various magnets used to manipulate the direction of the proton polarization. In addition, subtle geometrical biases in the data were more important here than in I, because no correlation was required; thus, any bias enters linearly in this analysis, but quadratically in the previous one. A brief description of the theoretical formalism is followed below by a discussion of the experimental technique using the polarization steering magnets, and of the problems of analyzing the spark-chamber film.

II. NUCLEON POLARIZATION AND THE WOLFENSTEIN PARAMETERS

Transverse-polarized nucleon beams can be produced and analyzed by scatterings. For an unpolarized beam and target, symmetry requires that there be no azimuthal dependence to the differential-scattering cross section I_0 and invariance under the parity transformation requires that the only possible component of final polarization be normal to the scattering plane. Furthermore, the azimuthal asymmetry in the scattering of a polarized beam can be used to determine the transverse component of the beam polarization.⁹

Spin directions can be rotated with magnetic fields.¹⁰ If a beam of protons passes axially through a solenoidal magnetic field, the transverse component of polarization will precess around the solenoid axis. Bending magnets

* Work supported in part by the U. S. Office of Naval Research, under Contract No. Nonr-1858(06).

† Present address: Harvard University, Cambridge, Massachusetts.

‡ Present address: University of Wisconsin, Madison, Wisconsin.

¹ E. Engels, T. Bowen, J. W. Cronin, R. L. McIlwain, and L. G. Pondrom, Phys. Rev. **129**, 1858 (1963). Hereafter referred to as I.

² L. Wolfenstein Phys. Rev. **96**, 1654 (1954).

³ R. Wilson, *The Nucleon-Nucleon Interaction, Experimental and Phenomenological Aspects* (Interscience Publishers, Inc., New York, 1963).

⁴ L. Wolfenstein, Ann. Rev. Nucl. Sci. **6**, 43 (1956).

⁵ W. N. Hess, Rev. Mod. Phys. **30**, 368 (1958).

⁶ M. H. MacGregor, M. J. Moravcsik, and H. P. Stapp, Ann. Rev. Nucl. Sci. **10**, 291 (1960).

⁷ G. Breit, Rev. Mod. Phys. **34**, 766 (1962).

⁸ B. P. Nigam, Rev. Mod. Phys. **35**, 117 (1963).

⁹ L. Wolfenstein, Phys. Rev. **75**, 1664 (1949).

¹⁰ V. Bargmann, L. Michel, and V. L. Telegdi, Phys. Rev. Letters **2**, 435 (1959).

can be used to rotate polarization components from longitudinal to transverse and vice versa, because the anomalous magnetic moment of the proton causes the spin and momentum vectors to precess at different rates.

Thus one is able to prepare a beam with any desired orientation of polarization by scattering an unpolarized beam and using a solenoid and/or a bending magnet to change the orientation of $\langle\sigma\rangle$. Furthermore, any component of an unknown polarization can be analyzed: the transverse component by scattering and the longitudinal component by converting it to transverse polarization in a bending magnet and then scattering. Three scatterings are required to study the effect of the p - p interaction on the polarization; the first prepares the polarized beam, the second alters the polarization via the interaction under study, and the third analyzes the altered polarization.

To describe the p - p scattering in the laboratory, let \mathbf{k}_i and \mathbf{k}_f be the initial and final momenta, and $\mathbf{n}_i = \mathbf{k}_i \times \mathbf{k}_f$ the normal to the scattering plane. The initial beam polarization is referred to an orthogonal triad of unit vectors $(\hat{k}_i, \hat{s}_i, \hat{n}_i)$ where $\mathbf{s}_i = \mathbf{n}_i \times \mathbf{k}_i$. Similarly, the final polarization is referred to the triad $(\hat{k}_f, \hat{s}_f, \hat{n}_f)$ where $\mathbf{n}_f = \mathbf{n}_i$ and $\mathbf{s}_f = \mathbf{n}_f \times \mathbf{k}_f$. The scattering angle is θ where $\cos\theta = \hat{k}_i \cdot \hat{k}_f$. Invariance arguments then show that $\langle\sigma_f\rangle$ can be expressed as

$$I_p(\theta, \phi) \langle\sigma_f\rangle = I_0(\theta) [(P + D \langle\sigma_i \cdot \hat{n}_i\rangle) \hat{n}_f + (A \langle\sigma_i \cdot \hat{k}_i\rangle + R \langle\sigma_i \cdot \hat{s}_i\rangle) \hat{s}_f + (A' \langle\sigma_i \cdot \hat{k}_i\rangle + R' \langle\sigma_i \cdot \hat{s}_i\rangle) \hat{k}_f], \quad (1)$$

where $I_p(\theta, \phi)$ and $I_0(\theta)$ are the differential scattering cross sections for a polarized and unpolarized beam, respectively. The parameters P , D , A , R , A' , and R' are functions only of θ and the energy E .

To measure P , R , and R' a beam of protons is prepared with a net polarization P_1 in the direction \hat{s}_i . Then Eq. (1) reduces to

$$\langle\sigma_f\rangle = P \hat{n}_f + R' P_1 \hat{k}_f + R P_1 \hat{s}_f. \quad (2)$$

Using a spark chamber as an analyzer of transverse polarization, $\langle\sigma_f \cdot \hat{n}_f\rangle$ and $\langle\sigma_f \cdot \hat{s}_f\rangle$. If prior to scattering $\langle\sigma_f\rangle$ is rotated by 90° around \hat{n}_f , then $\langle\sigma_f \cdot \hat{k}_f\rangle$ can also be measured. These expectation values are related to the triple scattering parameters R and R' by the following formulas:

$$\begin{aligned} \langle\sigma_f \cdot \hat{n}_f\rangle &= P, \\ \langle\sigma_f \cdot \hat{s}_f\rangle &= R P_1, \\ \langle\sigma_f \cdot \hat{k}_f\rangle &= R' P_1. \end{aligned} \quad (3)$$

Similarly, if a beam is prepared with polarization P_1 in the direction of \hat{k}_i , then

$$\langle\sigma_f\rangle = P \hat{n}_f + A' P_1 \hat{k}_f + A P_1 \hat{s}_f. \quad (4)$$

The measurable transverse components of the final polarization are the same three as above and are related

to P , A , and A' by the formulas

$$\begin{aligned} \langle\sigma_f \cdot \hat{n}_f\rangle &= P, \\ \langle\sigma_f \cdot \hat{s}_f\rangle &= A P_1, \\ \langle\sigma_f \cdot \hat{k}_f\rangle &= A' P_1. \end{aligned} \quad (5)$$

Again, a rotation of the final spin is required to measure

$$\langle\sigma_f \cdot \hat{k}_f\rangle.$$

To measure D , a beam is prepared with polarization along \hat{n}_i . Then Eq. (1) reduces to

$$(1 + \mathbf{P}_1 \cdot \mathbf{P}) \langle\sigma_f\rangle = \langle P + D \mathbf{P}_1 \cdot \hat{n}_i \rangle \hat{n}_i, \quad (6)$$

where the term, $(1 + \mathbf{P}_1 \cdot \mathbf{P})$, is the ratio I_p/I_0 , for \mathbf{P}_1 along \hat{n}_i . The measurable transverse component of polarization is

$$\langle\sigma_f \cdot \hat{n}_f\rangle = (P + D P_1) / (1 + \mathbf{P}_1 \cdot \mathbf{P}). \quad (7)$$

From this and the value of P the parameter D can be determined.

Defined in this way, the triple-scattering parameters can be directly measured in the laboratory. The parameters can be related to the nucleon-nucleon scattering matrix elements, and hence to the phase shifts, by direct calculation in the c.m. system. A nonrelativistic transformation into the lab then mixes the coefficients in the plane of scattering (R and A for example) in a simple way. Relativistic corrections must be applied at high energies. In this paper we always consider the parameters defined in the laboratory. The predictions based on phase-shift analyses with which the data are compared have, therefore, been appropriately transformed.

III. EXPERIMENTAL APPARATUS

A. Polarized Beam and Hydrogen Target

The polarized beam was produced by scattering the internal beam of the University of Chicago synchrocyclotron from a beryllium target $\frac{1}{4}$ in. long and $\frac{1}{16}$ in. high. The central orbit corresponded to 13.5° left scattering in the median plane. Two triplet strong focusing magnets were used to transport the beam 60 ft to the hydrogen target. The full width at half-maximum of the beam at the hydrogen target was $\frac{5}{8}$ in. vertically and $1\frac{1}{4}$ in. horizontally. The beam pulse was 0.3 msec long, and appeared at 60 cps. The average beam intensity was 5×10^7 /sec. The hydrogen target was similar to the one used in I. The target cup was 5.5 in. in diameter and 5.75 in. high and presented 0.007-in. Mylar walls to the incoming and scattered beam. The vacuum jacket windows were also 0.007-in. Mylar. The target was so designed that it could be filled or emptied in about 1 min.

B. Triggering Scheme and Rates

Figure 1 shows the arrangement of scintillation counters used to detect triple-scattering events. Counters C_1 , C_2 , and C_3 were connected in coincidence and C_4 in

anticoincidence. Protons scattering in the horizontal plane through an angle θ_L from the hydrogen target were detected in the 2-in. \times 2-in. \times $\frac{1}{8}$ -in. counter C_1 . A count in C_2 assured that the scattered proton traversed the spark chamber without scattering through an angle greater than 40° . The anticoincidence counter \bar{C}_4 subtended a polar angle of 5° at the center of the spark chamber and hence rejected events in which the proton to be analyzed either did not scatter in the spark chamber or scattered through an angle smaller than 5° . The range of polar angles used in the data analysis was 9° - 27° , just within the angular triggering range defined by C_2 and \bar{C}_4 . C_3 was a 6-in. \times 6-in. counter which detected the recoil proton from elastic p - p scatterings in the target. With five carbon plates $\frac{1}{2}$ in. thick in the spark chamber, about 10% of the $C_1 C_2 C_3$ counts satisfied $C_1 C_2 C_3 \bar{C}_4$. For the measurement of A' , the separation between the hydrogen target and C_1 was lengthened by the presence of the A' magnet and the layout was altered to that shown in Fig. 4. The four counters were timed and plateaued at each scattering angle. Particular attention was paid to the efficiency of C_2 , because of possible false asymmetry effects. The spark-chamber control circuitry has been described in detail by Cronin and Renninger¹¹ and in I. A dead time limited the picture-taking rate to 6/sec.

The beam normalization for all counting rates was provided by an ionization chamber with a calibration of 1.2×10^9 protons/V. The total rate of C_{123} coincidences represented the elastic-scattering rate plus the rates of background and accidentals. Figure 2 shows the observed C_{123} rate versus the center-of-mass angle θ^* . The " $P_1 \perp \hat{n}$ " was obtained by transforming the isotropic distribution $I_0(\theta^*) = 4$ mb/sr into the lab and using the appropriate lab solid angle and proton monitor

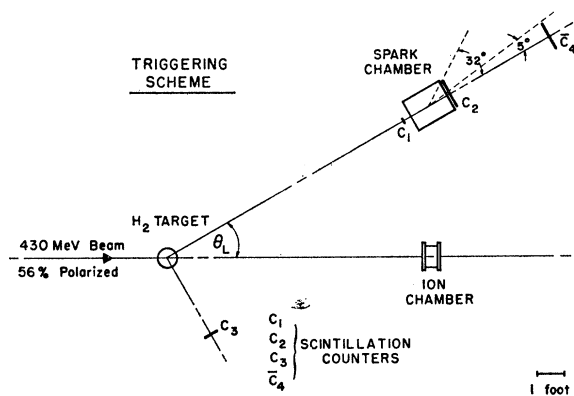


FIG. 1. Layout of the scintillation counters, ion-chamber monitor, and spark chamber. The disposition of the polarization steering magnets is shown in Fig. 4. For A' a second bending magnet was inserted between the hydrogen target and the spark chamber.

¹¹ J. W. Cronin and G. Renninger, in Proceedings of an International Conference on Instrumentation for High Energy Physics, 1960, Lawrence Radiation Laboratory, 1960 (unpublished).

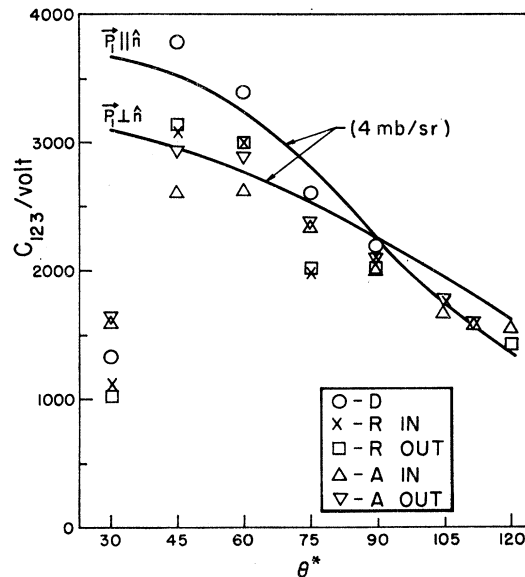


FIG. 2. Absolute efficiency of the 123 coincidence rates for observing p - p scattering. The ordinate is the number of coincidences normalized to the proton-beam monitor. See text for the notation used to label the points.

calibrations. The curve " $P_1 \parallel \hat{n}$ " was obtained by transforming $I_0(\theta^*)[1 + P_1 P_2(\theta^*)]$ into the lab. This expression is suitable for comparison with the D rates. The fit is good except at $\theta^* = 30^\circ$, where the detection efficiency for the recoil protons was poor. This indicates that the counter telescope operated with good efficiency for detecting p - p scattering events.

IV. EXPERIMENTAL PROCEDURE

A. Calibration of Polarization Detector

If a proton incident along $+z$ has polarization P in the $+y$ direction, the scattering from a carbon plate has an azimuthal dependence of the form $(1 + \epsilon \cos \phi)$, where ϕ is the azimuthal angle of the scattered proton with respect to the x axis in a right-handed system, and ϵ is a constant proportional to the polarization P . The constant of proportionality P_3 is interpreted as the analyzing power of the spark chamber. P_3 is a function of incident-proton energy and polar scattering angle Θ . The Θ dependence was averaged in the range 9° - 27° in the data analysis. For the measurement of R , A , and A' it was only necessary to know the product, $\epsilon_C(E_i) = P_1 P_3(E_i)$. This quantity ϵ_C was directly measured by placing the spark chamber in the polarized proton beam with several different thicknesses of nondepolarizing carbon absorber. The details of the analysis will be given in Sec. V, but the results are shown in Fig. 3, where $P_1 \times P_3$ is plotted versus the incident-proton energy. The polarization P_1 of the Chicago beam was determined with respect to the well-known polarization, $P_R = 0.89 \pm 0.02$, of the Rochester beam by using the data in I, where $P_R \times P_3(210 \text{ MeV})$ was measured. Then

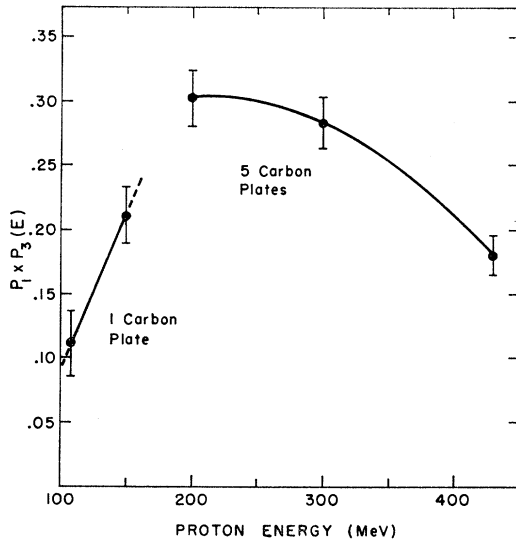


FIG. 3. Carbon-plate spark-chamber calibration. $P_3(E)$ is the energy-dependent analyzing power of the spark chamber in the range of lab angles from 9° to 27° . P_1 is the polarization of the proton beam in which these data were obtained. The carbon plates were $\frac{1}{2}$ in. thick.

the polarization of the Chicago beam was computed using the product $P_1 \times P_3(210 \text{ MeV}) = 0.309\% \pm 0.020$ from Fig. 3, as follows:

$$P_1 = P_1 P_3(210) / P_R P_3(210) \times P_R = 0.56 \pm 0.04. \quad (8)$$

Using Fig. 3 and the calculated value of the Chicago polarization, the analyzing power of the chamber for any incident energy in the range 100–430 MeV can be calculated. However, P_3 itself was necessary only for the calculation of P and D , and in these calculations it was entered as the ratio ϵ_C/P_1 . This was done to simplify the combination of errors. Thus the formulas for D and P as used for computations are

$$D = \frac{\epsilon_D(1 + P_1^2 \epsilon_P / \epsilon_C) - \epsilon_P}{\epsilon_C}, \quad (9)$$

and

$$P = \epsilon_P P_1 / \epsilon_C, \quad (10)$$

where ϵ_D and ϵ_P are the left-right asymmetries measured with the component of incident polarization perpendicular to the scattering plane equal to P_1 and zero, respectively.

It was convenient to measure D and R sequentially at each scattering angle because no repositioning of apparatus was required. The experimental arrangement for the measurement of D and R is shown in Fig. 4. For the measurement of D , the solenoid was turned off. Thus the direction of polarization of the beam incident on the hydrogen target was normal to the scattering plane. For measuring R , the current in the 700-turn solenoid necessary to rotate the polarization by 90° was 2165 A. This current was regulated to $\pm \frac{1}{2}\%$. The spark

chamber was mounted on a cart attached to a 10-ft I-beam pivoted below the center of the hydrogen target. The cart was positioned to better than $3'$ of arc at each of the seven scattering angles by using a telescope mounted on the beam line and a mirror mounted on a rotating plate attached to the pivot. To take data at each angle the counters were first re-turned, and the rates of elastic scattering, background, and accidentals were checked. Then 17 000 to 20 000 photographs were taken for each of the configurations D , $R-I$, and $R-O$, where I and O correspond to an axial magnetic field "in" or "out" of the solenoid, giving clockwise or counter-clockwise rotation of the beam polarization. The double measurement of R was designed to eliminate the effect of up-down biases in the apparatus or analysis procedure. For the largest two scattering angles, 50° and 57° , a one-carbon-plate assembly was used instead of the usual five-plate assembly and more events were photographed to compensate for the low proton energies and smaller analyzing power at these scattering angles.

For the measurement of the parameter A , it was necessary to produce an incident beam with its polarization vector along the direction of motion. This was done with two magnets as shown in the upper right section of Fig. 4. First the solenoid described above was used to rotate the polarization clockwise (or counter-clockwise) into the horizontal plane, perpendicular to the direction of motion. Then the polarization was rotated forward (or backward) into the direction of motion. This latter rotation utilized a bending magnet, the A magnet, which had the effect of rotating the momentum through an angle

$$\theta_B = \frac{e}{pc} \int \mathbf{B} \cdot d\mathbf{l}, \quad (11)$$

while at the same time rotating the polarization through a larger angle¹⁰

$$\theta_S = [1 + (\mu_p - 1)\gamma] \left(\frac{e}{pc} \right) \int \mathbf{B} \cdot d\mathbf{l}. \quad (12)$$

These two equations may be combined to form

$$\theta_S - \theta_B = (\mu_p - 1)\gamma\theta_B, \quad (13)$$

where γ is the proton energy measured in units of Mc^2 and μ_p is the proton magnetic moment in nuclear magnetons. Thus by choosing $(\theta_S - \theta_B) = \frac{1}{2}\pi$, we could align the polarization with the direction of motion of the beam protons as required for the measurement of A . For 430-MeV incident protons, the necessary bending angle was 34.5° . The spark chamber and recoil counter were positioned at each scattering angle as described for D and R , and data taking for $A-I$ and $A-O$ proceeded just as for $R-I$ and $R-O$.

The arrangement of the spark chamber, magnets, target, and counters used to measure A' is also shown in Fig. 4. The solenoid, A magnet, and target were

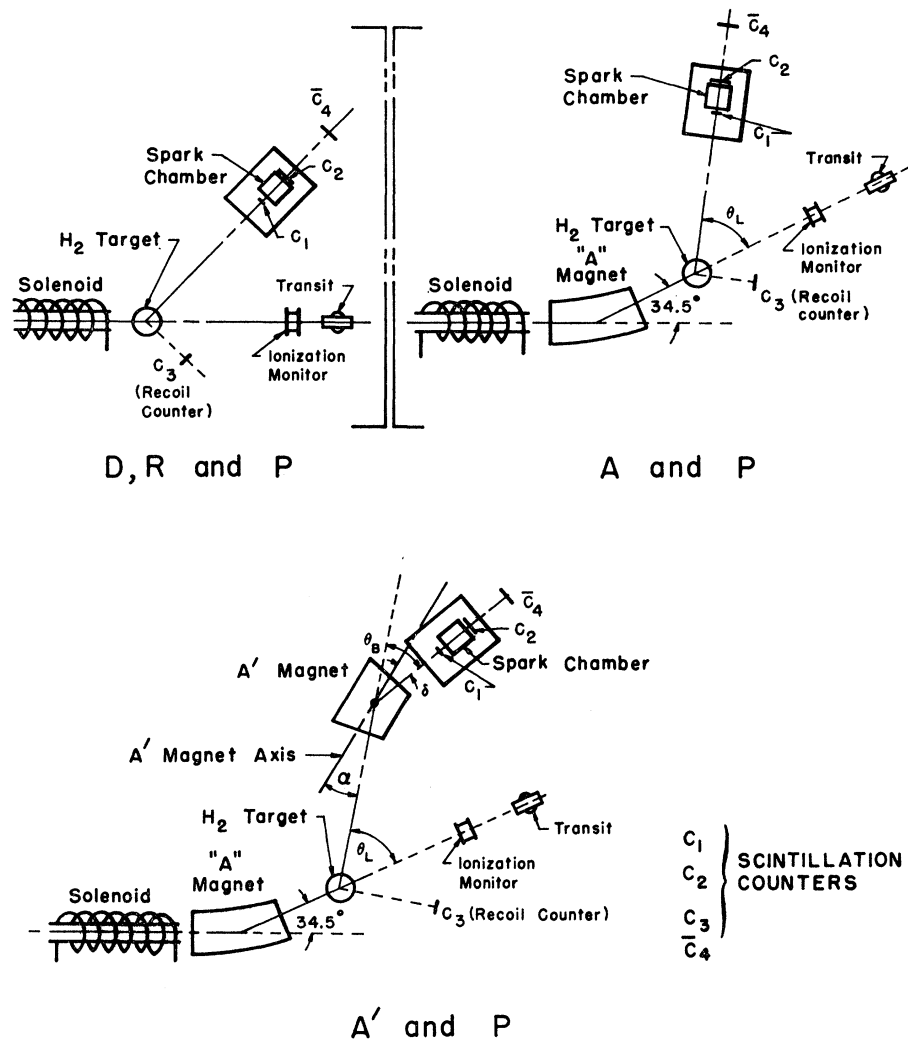


FIG. 4. Floor layouts for the various parameter measurements. The figures represent the horizontal plane. The solenoid was used to rotate the vertical proton spin into the horizontal plane. The *A* magnet then rotated the spin to make it longitudinal. The *A'* magnet rotated the longitudinal component of the spin into the transverse direction.

positioned exactly as they had been for the measurement of *A*. The *A'* magnet was mounted on a turntable bolted to an I-beam pivoted beneath the hydrogen target. The spark chamber cart was bolted to a second I-beam pivoted beneath the center of the *A'* magnet. For each of the seven scattering angles at which *A'* was measured it was necessary to reposition the *A'* magnet and the spark chamber. The settings are specified by the angles α , $\alpha = \delta = \frac{1}{2}\theta_B$, and θ_L as shown in Fig. 4, where α and δ are the entrance and exit angles to the *A'* magnet for protons scattering at an angle θ_L from the hydrogen target.

The current in the *A'* magnet was set so that protons scattering elastically at an angle θ_L in the hydrogen target were bent through the angle θ_B necessary to satisfy $(\theta_S - \theta_B) = \frac{1}{2}\pi$. After the geometry was optically set, the current was varied in the *A'* magnet until the C_{123} coincidence rate was maximized. Since C_3 and the telescope C_1 - C_2 were at the kinematically correct

angles to detect elastic p - p events, we were then assured that the $\int \mathbf{B} \cdot d\mathbf{l}$ was properly set.

V. DATA ANALYSIS

The scanning criteria for the spark chamber film were exactly the same as those applied in I, using angle encoders of the same $\frac{1}{3}^\circ$ least count. An event was rejected if the incident proton was not normal to the chamber to within 1° , if the scatter did not occur in carbon, or if extra sparks were associated with the scattering vertex.

Before the measuring table output could be used to calculate the scattering asymmetries, certain corrections had to be incorporated. The effects of magnification in the cylindrical lens used in the optics, parallax, and projection on a flat screen were included in the analysis. In addition, the effects of slight misalignments that occurred during changes of the carbon plates in the spark chamber were also taken into account.

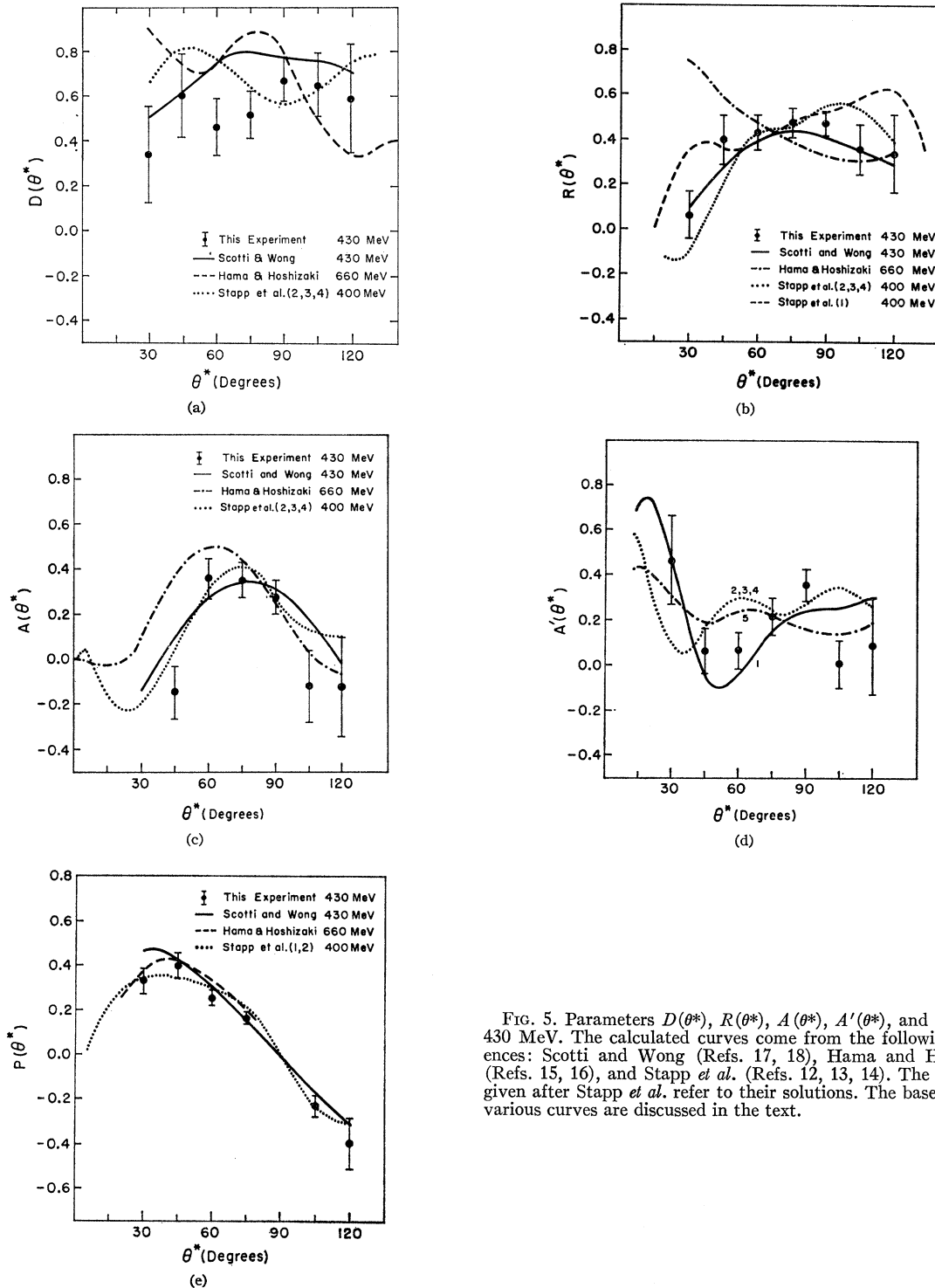


FIG. 5. Parameters $D(\theta^*)$, $R(\theta^*)$, $A(\theta^*)$, $A'(\theta^*)$, and $P(\theta^*)$ at 430 MeV. The calculated curves come from the following references: Scotti and Wong (Refs. 17, 18), Hama and Hoshizaki (Refs. 15, 16), and Stapp *et al.* (Refs. 12, 13, 14). The numbers given after Stapp *et al.* refer to their solutions. The bases for the various curves are discussed in the text.

For protons incident along the z axis with $\langle \sigma \rangle_1$ making an angle ϕ_0 with the positive x axis, the scattering distribution in spark chamber plates will have the form

$$P(\phi) = 1 + \epsilon \cos(\phi - \phi_0 + \frac{1}{2}\pi), \quad (14)$$

where ϵ , the asymmetry parameter, is proportional to $\langle \sigma \rangle_1$ and ϕ is the azimuthal angle of scattering. The maximum-likelihood estimates of the horizontal and vertical components ϵ_x and ϵ_y of ϵ , where

$$\epsilon_x = \epsilon \cos(\phi_0 - \frac{1}{2}\pi), \quad \epsilon_y = \epsilon \sin(\phi_0 - \frac{1}{2}\pi) \quad (15)$$

TABLE I. Asymmetries before bias correction.

Parameter	θ_L	Up-down asymmetries		
		Solenoid field direction		
		In	Out	
R	13°	0.153±0.032	0.126±0.030	
R	20°	0.175±0.031	-0.011±0.032	
R	27°	0.231±0.030	-0.001±0.028	
R	35°	0.188±0.025	-0.091±0.025	
R	42°	0.220±0.018	-0.064±0.016	
R	50°	0.123±0.036	-0.044±0.032	
R	57°	0.074±0.025	0.002±0.023	
A	13°	-0.052±0.044	0.053±0.046	
A	20°	0.088±0.035	0.018±0.040	
A	27°	0.006±0.033	0.201±0.034	
A	35°	-0.033±0.027	0.173±0.032	
A	42°	-0.009±0.029	0.157±0.030	
A	50°	0.024±0.055	-0.032±0.052	
A	57°	0.028±0.027	0.002±0.037	
A'	13°	-0.085±0.045	0.109±0.064	
A'	20°	0.031±0.030	0.061±0.037	
A'	27°	0.054±0.032	0.020±0.032	
A'	35°	0.122±0.032	-0.005±0.033	
A'	42°	0.159±0.030	-0.055±0.029	
A'	50°	0.010±0.035	0.008±0.037	
A'	57°	0.045±0.032	0.028±0.033	
200 C		-0.097±0.027	-0.035±0.024	
θ_L	Left-right asymmetries			
	ϵ_P	ϵ_D	Energy	ϵ_C
13°	0.079±0.017	0.120±0.034	109 C	0.045±0.028
20°	0.122±0.015	0.207±0.031	150 C	0.145±0.026
27°	0.079±0.013	0.174±0.026	200 C	0.235±0.024
35°	0.042±0.012	0.175±0.025	300 C	0.217±0.023
42°	-0.044±0.011	0.160±0.023	430 C	0.115±0.018
50°	-0.140±0.016	0.022±0.029	200 C-I	-0.097±0.027
57°	-0.120±0.012	-0.060±0.023	200 C-O	-0.035±0.024

were found separately for the events in each 400-ft roll of film. Since $|\epsilon|$ was less than 0.25 in all cases the estimates and their dispersions were calculated from the following formulas:

$$\epsilon_x = \langle \cos\phi \rangle / \langle \cos^2\phi \rangle, \quad \epsilon_y = \langle \sin\theta \rangle / \langle \sin^2\phi \rangle, \quad (16)$$

$$\sigma^2_{\epsilon_x} = 1/n \langle \cos^2\phi \rangle, \quad \sigma^2_{\epsilon_y} = 1/n \langle \sin^2\phi \rangle.$$

The cross correlation was negligible; the averages were taken over the n events in each roll. The errors from the scanning and measuring process, determined by scanning some rolls several times, increased the statistical errors by 20–40%.

The slight misalignments in the optical system mentioned above contributed some small up-down and

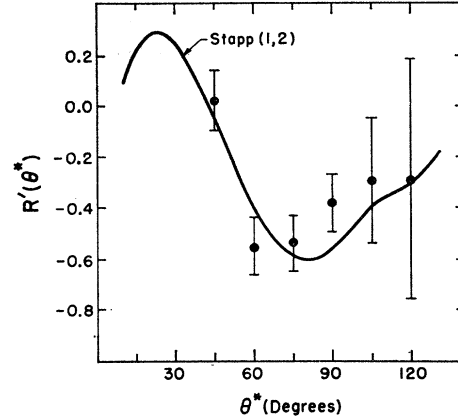


FIG. 6. Parameter $R'(\theta^*)$ calculated from our R , A , and A' data. The numbers refer to solutions of Stapp *et al.* for R' at 400 MeV.

right-left biases to the data. As can be seen from Table I, however, a bias favoring “up” over “down” remained in the data, as did a bias favoring “right” over “left.” These biases amounted to asymmetries of approximately 0.05. Although the reasons for these biases are not understood, the data were taken in a way in which the biases could be eliminated. The up-down bias could be subtracted out by combining the two asymmetries observed for the solenoid magnetic field parallel and antiparallel to the incident proton line of flight. Calling these asymmetries ϵ_I and ϵ_0 , ϵ_I should equal $-\epsilon_0$ in the absence of a geometrical bias. To eliminate the bias we formed $\epsilon = \frac{1}{2}(\epsilon_I - \epsilon_0)$. The corrected values of ϵ are shown in Table II. The left-right bias could be obtained from the R , A , and A' right-left asymmetries observed at $\theta^* = 90^\circ$, where $P_2(\theta^*) = 0$, and from some 200-MeV calibration data taken with the spark chamber in the direct beam with the solenoid energized. The latter data are the last two right-left asymmetries in Table I. For none of these cases should a right-left asymmetry exist in the absence of bias. From the calibration data a bias of -0.066 ± 0.018 was found favoring right scattering, and this bias was subtracted from all calibration data shown in Fig. 3; interpolated values of P_1P_3 are given in Table II. From the right-left asymmetries observed at $\theta^* = 90^\circ$ a bias of -0.044 ± 0.011 was found, and was subtracted from the measured right-left asymmetries in the P and D data. These corrected numbers are given in Table II. Both corrections were for 200

TABLE II. Final asymmetries.

θ^*	ϵ_R	ϵ_A	$\epsilon_{A'}$	ϵ_D	ϵ_P	$\epsilon_{P_1P_3}$
30°	0.013±0.022	0.053±0.032	0.097±0.039	0.164±0.034	0.123±0.017	0.208±0.020
45°	0.093±0.023	-0.035±0.027	0.015±0.024	0.251±0.031	0.166±0.015	0.234±0.025
60°	0.116±0.020	0.097±0.023	0.017±0.023	0.218±0.026	0.122±0.014	0.271±0.022
75°	0.139±0.018	0.103±0.021	0.063±0.023	0.219±0.025	0.086±0.013	0.294±0.022
90°	0.142±0.012	0.083±0.021	0.107±0.021	0.204±0.023	0.000±0.012	0.302±0.020
105°	0.083±0.024	-0.028±0.038	0.001±0.025	0.066±0.029	-0.096±0.017	0.235±0.025
120°	0.036±0.017	-0.013±0.023	0.009±0.023	-0.016±0.023	-0.016±0.012	0.107±0.025

MeV only, but the bias was assumed to be energy independent. This assumption could be verified for the up-down biases, where data at all energies were available.

The calculation of the triple scattering parameters from the corrected asymmetries was then a simple matter, using the equations

$$\begin{aligned} R &= \epsilon_R / \epsilon_C, \\ A &= \epsilon_A / \epsilon_C, \\ A' &= \epsilon_{A'} / \epsilon_C, \end{aligned} \quad (17)$$

together with Eqs. (9) and (10). Table III gives the final results, together with the standard-deviation errors.

TABLE III. Polarization parameters at 430 MeV.

$\theta_{e.m.}$	D	R	A	A'	P
30°	0.34 ± 0.22	0.06 ± 0.11	0.25 ± 0.16	0.47 ± 0.20	0.33 ± 0.06
45°	0.60 ± 0.19	0.40 ± 0.11	-0.15 ± 0.12	0.06 ± 0.11	0.40 ± 0.06
60°	0.47 ± 0.13	0.43 ± 0.08	0.36 ± 0.09	0.06 ± 0.09	0.25 ± 0.04
75°	0.52 ± 0.11	0.47 ± 0.07	0.35 ± 0.08	0.22 ± 0.08	0.16 ± 0.03
90°	0.67 ± 0.10	0.47 ± 0.05	0.27 ± 0.07	0.36 ± 0.07	0.00 ± 0.02
105°	0.65 ± 0.15	0.35 ± 0.11	-0.12 ± 0.16	0.01 ± 0.11	-0.23 ± 0.05
120°	0.59 ± 0.25	0.34 ± 0.18	-0.12 ± 0.22	0.08 ± 0.04	-0.40 ± 0.11

VI. RESULTS

The data in Table III are plotted in Fig. 5. Curves representing various predictions are shown for comparison. Stapp, Noyes, and Moravcsik^{12,13} have made an energy-dependent phase-shift analysis using 423 pieces of data in the energy range 10–385 MeV. They obtained several possible solutions all of similar character. The five best solutions have been extrapolated to 400 MeV.¹⁴ These solutions are all combined as one curve on the figures when the differences between them are small compared to experimental error. Hama and Hoshizaki¹⁵ and Hoshizaki and Machida¹⁶ performed a phase shift analysis of Dubna data at 660 MeV, using a total of

¹² H. P. Stapp, M. J. Moravcsik, and H. P. Noyes, in *Proceedings of the 1960 Annual International Conference on High Energy Physics at Rochester*, edited by E. C. G. Sudarshan, J. H. Tinlot, and A. C. Melissinos (Interscience Publishers, Inc., New York, 1960), p. 132.

¹³ H. P. Stapp, H. P. Noyes, and M. J. Moravcsik, in *Proceedings of the 1962 International Conference on High Energy Physics at CERN*, edited by J. Prentke (CERN, Geneva, 1962), p. 131.

¹⁴ R. Arndt (private communication).

¹⁵ Y. Hama and N. Hoshizaki, Research Institute for Fundamental Physics, Kyoto, Report No. 30, 1963 (unpublished).

¹⁶ N. Hoshizaki and S. Machida, *Progr. Theoret. Phys.* (Kyoto) **29**, 49 (1963).

45 data points. Their fits are plotted directly with our experimental results. The 660-MeV data were in the c.m. range 55° to 125°, and the fit agrees with our results in this range, but the agreement is poor at 30° and 45°. The third analysis with which the data are compared is a phenomenological model by Scotti and Wong.¹⁷ In this model, the pion resonances up to about 1 BeV are introduced into the framework of a dispersion-theoretic calculation of nucleon-nucleon scattering. In addition to the usual one-pion exchange, the exchanges of η , ω , ρ , ϕ , and an S -wave pion-pion pair are introduced. The search was then in terms of coupling constants, masses, and Regge cutoffs. About 500 experimental data points below 385 MeV were used for the search and the resulting fits have been extrapolated¹⁸ to our energy, 430 MeV. The fits are in good agreement with our data and the model itself is conceptually appealing.

Figure 6 shows the triple scattering parameter $R'(\theta^*)$ calculated from our data on A and R using Sprung's¹⁹ relativistic relation

$$\tan\theta_L = (A + R') / (A' - R). \quad (18)$$

The data are compared with the prediction based on Stapp's extrapolation to 400 MeV. The fit is good but the experimental errors are quite large. Stapp's predictions of course satisfy the same Eq. (18), but the good agreement with the experimental data adds credence to the lack of systematic biases in our final values of R , A , and A' .

ACKNOWLEDGMENTS

We wish to thank the staff of the Chicago synchro-cyclotron for its support during the experiment. Professor J. Cronin gave continued guidance and support. James Christenson, Paul Kirk, and Wayne Vernon helped during the run. The scanners at Columbia and in particular Mrs. D. Josephine Elms and her co-workers at Princeton carefully measured 500 000 events. Extensive use was made of the Princeton Computer Center, supported by the National Science Foundation. Professor Antonio Scotti and Dr. Richard Arndt provided extrapolated predictions from their analyses of data at lower energies.

¹⁷ A. Scotti and D. Y. Wong, *Phys. Rev. Letters* **10**, 142 (1963).

¹⁸ A. Scotti (private communication).

¹⁹ D. W. L. Sprung, *Phys. Rev.* **121**, 925 (1961).